Importance of molecular Rayleigh scattering in the enhancement of clear sky reflectance in the vicinity of boundary layer cumulus clouds

Guoyong Wen,[1,2] Alexander Marshak,[1] and Robert F. Cahalan[1]

[1] Clouds increase the complexity of atmospheric radiative transfer processes, particularly for aerosol retrievals in clear regions in the vicinity of clouds. This study focuses on identifying mechanisms responsible for the enhancement of nadir reflectance in clear regions in the vicinity of cumulus clouds and quantifies the relative importance of each mechanism. Using cloud optical properties and surface albedo derived from Advanced Spaceborne Thermal Emission and Reflection Radiometer (ASTER) and Moderate Resolution Imaging Spectroradiometer (MODIS), we performed extensive Monte Carlo simulations of radiative transfer in two cumulus scenes in a biomass burning region in Brazil. The results show that the scattering of radiation by clouds, followed by upward Rayleigh scattering by molecules above cloud top over clear gaps, is the dominant mechanism for the enhancement of visible reflectance in clear regions in boundary layer cumulus field over dark surfaces with aerosols trapped in the boundary layer. The Rayleigh scattering contributes $\sim$80% and $\sim$50% to the total enhancement for wavelengths 0.47 μm (with aerosol optical thickness 0.2) and 0.66 μm (with aerosol optical thickness 0.1), respectively. Out of the total contribution of molecular scattering, $\sim$90% arises from the clear atmosphere above cloud top height. The mechanism is valid for a large range of aerosol optical thicknesses (up to 1 in this study) for 0.47 μm, and for aerosol optical thickness up to 0.2 for 0.66 μm. Our results provide a basis to develop simplifications for future aerosol remote sensing from satellite.

Citation: Wen, G., A. Marshak, and R. F. Cahalan (2008), Importance of molecular Rayleigh scattering in the enhancement of clear sky reflectance in the vicinity of boundary layer cumulus clouds, *J. Geophys. Res.*, *113*, D24207, doi:10.1029/2008JD010592.

1. Introduction

[2] Aerosol and cloud are two important components of the Earth's atmosphere. Understanding the interaction between aerosols and clouds is particularly important in studying the direct and indirect effects of aerosols on climate as well as cloud processes. Satellite observations provide a unique opportunity to study aerosol and cloud interactions on a global scale. Efforts have been made to study the relationship between aerosol optical thickness and cloud properties [e.g., *Sekiguchi et al.*, 2003; *Loeb and Manalo-Smith*, 2005; *Zhang et al.*, 2005; *Ignatov et al.*, 2005; *Kaufman et al.*, 2005; *Kaufman and Koren*, 2006]. *Koren et al.* [2007] recently reported a "twilight" zone near cloud edges, and commented that "the total aerosol direct forcing may be significantly higher than is currently estimated due to large contributions from this transition zone."

[3] Regions near cloud edges are important in studying aerosol and cloud interactions, and satellite observations are valuable to this research. However, using satellite observa-tions to effectively study aerosol-cloud interaction remains a challenge. One of the problems is that reflected sunlight in clear regions in the vicinity of clouds is affected by nearby clouds. Studies have shown that clouds increase the reflectance of nearby clear regions, leading to large biases in aerosol optical thickness retrievals from satellite observations [e.g., *Cahalan et al.*, 2001; *Wen et al.*, 2001; *Nikolaeva et al.*, 2005; *Wen et al.*, 2006, 2007; *Kassianov and Ovtchinnikov*, 2008; *Marshak et al.*, 2008; *Yang and Di Girolamo*, 2008].

[4] Our previous studies focused on quantifying the magnitude of the enhancement and associated bias in aerosol retrievals. This study is an extension of our previous work [*Wen et al.*, 2006, 2007] with an emphasis on identifying the physical mechanisms responsible for the reflectance enhancement. We will show that the scattering of radiation by clouds, followed by upward Rayleigh scattering by molecules above cloud top height is the dominant mechanism for the reflectance enhancement in clear regions in boundary layer cumulus fields. Such low clouds occur in large areas of the globe and provide a significant contribution to net cloud forcing [*Hartmann et al.*, 1992], and results of this work are significant to understanding the role of aerosol-cloud interactions on cloud forcing.

[5] In section 2, we briefly describe the aerosol and cloud properties used in the Monte Carlo simulation. Section 3

¹NASA Goddard Space Flight Center, Greenbelt, Maryland, USA.
²Goddard Earth Sciences and Technology Center, University of Maryland Baltimore County, Baltimore, Maryland, USA.
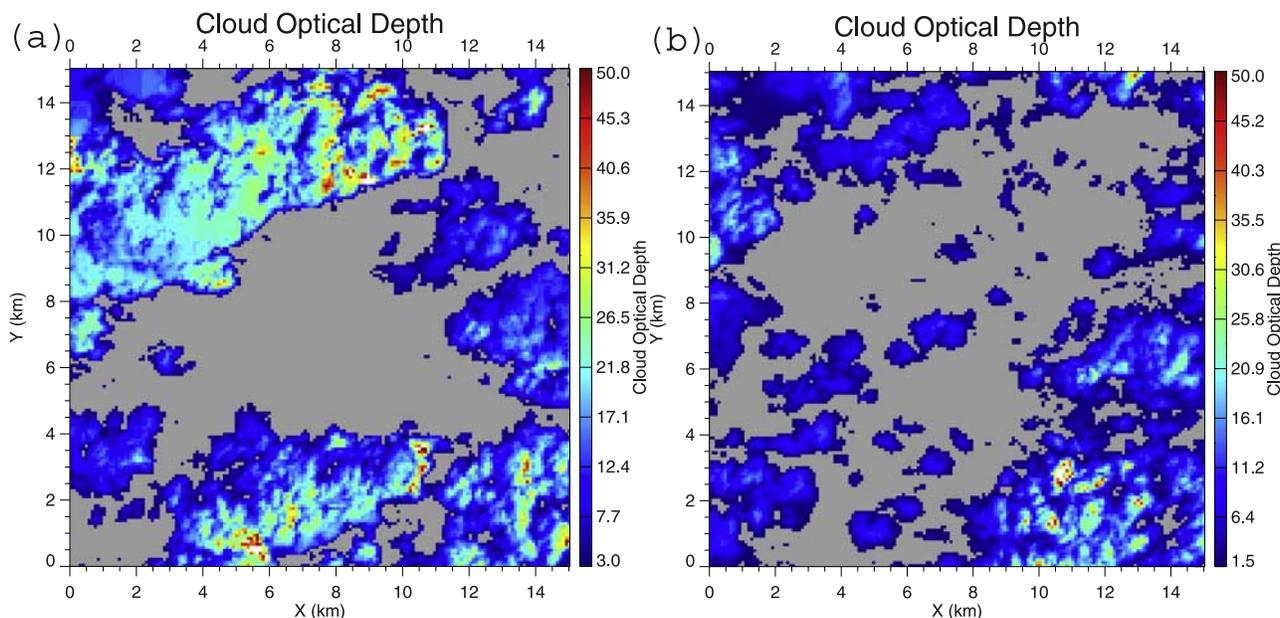
Figure 1. Cloud optical depth of (a) thick and (b) thin clouds. The average cloud optical depth is ~14 and ~7 with cloud cover of 59% and 51% for the thick and thin cloud, respectively.

describes our method of analysis. The results are presented in section 4 and summarized and discussed in section 5.

2. Cloud Fields and Aerosol Properties

[6] Two 15 km × 15 km high-resolution images of cumulus cloud fields are used in this study. They are subimages of an ASTER image collocated with a MODIS image acquired on 25 January 2003. The ASTER image is centered on the equator at 53.78°W with solar zenith angle (SZA) of 32° and solar azimuth angle of 129°. The same images were used by *Wen et al.* [2007] to study three-dimensional (3D) cloud effects on the reflectance enhancement in clear regions of cumulus scenes. The cloud optical depth of both images is retrieved from ASTER observations at 90-m resolution using a lookup table based on 1D radiative transfer similar to that for MODIS cloud retrieval [*Platnick et al.*, 2003]. The averaged cloud optical depths are 14 for the "thick" cloud and 7 for the "thin" cloud (Figure 1). The cloud fractions are 59% and 51% for thick and thin cloud, respectively. The cloud base is assumed to be constant at 1 km. Cloud top heights are estimated from brightness temperature at 11 μm (ASTER band 14) for both clouds. The average cloud top height is 1.5 km and 2 km for the thin clouds and thick clouds, respectively. The vertical profile of cloud liquid water is assumed to be proportional to the adiabatic liquid water content that is approximately a linear function of height [e.g., *Platnick*, 2000]. The phase function and single scattering albedo at the two MODIS bands, are computed assuming a gamma distribution of cloud droplets with an effective radius of 10 μm and an effective variance of 0.1 [e.g., *Hansen and Travis*, 1974]. The assumption of a constant droplet size is not really consistent with the adiabatic process. However, this simplification has no real consequences for the findings in this study.

[7] In biomass burning regions of Brazil, a strong trade wind inversion caps the shallow cumulus, and traps most aerosols in the atmospheric boundary layer [*Reid et al.*, 1998]. Here we assume that horizontally stratified aerosols are distributed in two distinctive vertical layers of the atmosphere: the boundary layer and the free troposphere. Most aerosols are trapped in the boundary layer, approximately 2 km thick. A small amount of aerosol, with optical thickness 0.01, is assumed in the free troposphere from 2 km to 10 km. We assume that aerosols are distributed uniformly in the vertical with a constant extinction in each layer. The model atmosphere is schematically shown in Figure 2a with cloud base and average cloud top heights indicated (Figure 2b). Aerosol particles are assumed to have a lognormal size distribution with a modal radius of 0.13 μm, a standard deviation of the natural logarithm of the radius of 0.6 and a single scattering albedo of 0.9, similar to the aerosol model in the MODIS aerosol algorithm [*Remer et al.*, 1998, 2005]. Aerosol phase functions are computed using Mie scattering theory. The aerosol phase function at 0.47 μm is presented in Figure 3 to compare with the Rayleigh scattering phase function for discussions in sections 4 and 5.

[8] The MODIS surface albedo product [*Moody et al.*, 2005] shows that the surface visible band reflectance is dark and homogeneous. So we use average surface albedos of 0.01 at 0.47 μm and 0.02 at 0.66 μm in this study.

[9] We use atmospheric and surface optical properties as inputs to the Goddard Monte Carlo (MC) code for radiative transfer in 3D cloudy atmospheres [*Evans and Marshak*, 2005]. This code has participated in all phases of Intercomparison of 3D Radiation Codes (I3RC) activities [*Cahalan et al.*, 2005]. The MC scheme uses the periodic condition in the horizontal and simulates the radiance in the nadir-viewing direction as observed by ASTER instrument.

3. Method

[10] Sunlight reaching Earth experiences scattering from molecules, aerosol particles, clouds, and surface reflection.
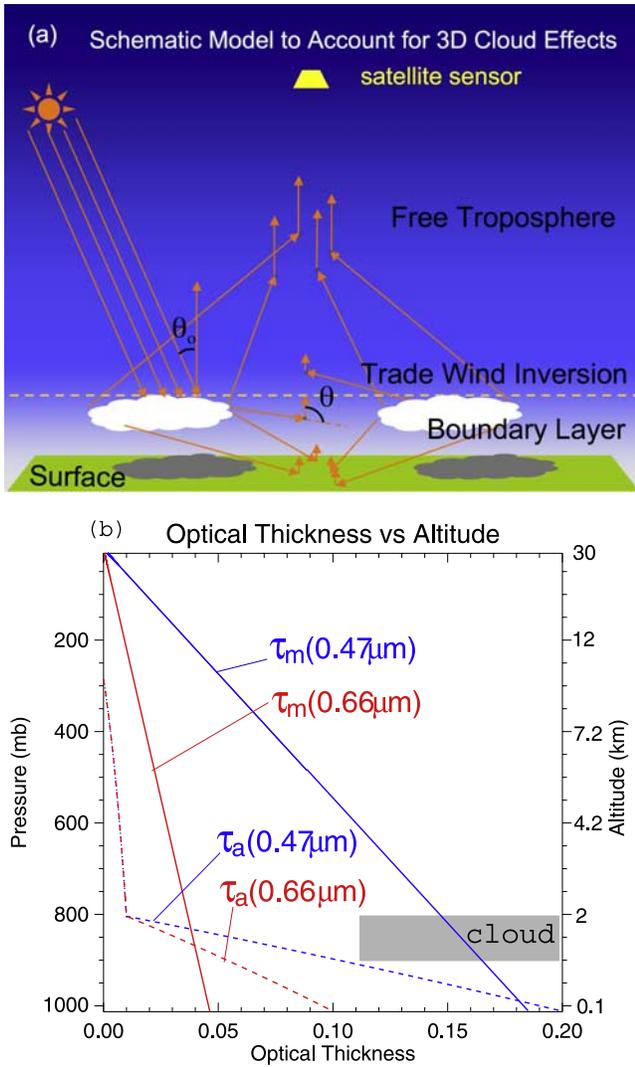
Figure 2. (a) Cumulus clouds and aerosols are trapped in the boundary layer owing to the trade wind inversion similar to that of *Reid et al.* [1998]. Solar zenith angle θ_o and the scattering angle θ are indicated. (b) Vertical distributions of molecular Rayleigh scattering optical thickness (τ_m) and aerosol optical thickness (τ_a) with cloud position indicated. The total optical thicknesses are $\tau_m(0.47\ \mu m) = 0.185$, $\tau_m(0.66\ \mu m) = 0.046$ and $\tau_a(0.47\ \mu m) = 0.2$, $\tau_a(0.66\ \mu m) = 0.1$. Above cloud top height molecular scattering optical thickness ($\tau_m(0.47\ \mu m) \sim 0.15$, $\tau_m(0.66\ \mu m) \sim 0.04$) are much larger than aerosol optical thickness ($\tau_a(0.47\ \mu m) \sim \tau_a(0.66\ \mu m) \sim 0.01$). The optical thickness is defined as $\tau = \int_{z}^{z_{TOA}} \beta(z)dz$, where β is the extinction coefficient.

Radiation received by an Earth-viewing satellite sensor is a sum of radiation scattered into the viewing direction from each layer of the atmosphere. Knowing the contribution from different layers of the atmosphere and from different scattering species is critical to understanding the radiative processes, remote sensing, and cloud effects on enhancing clear region reflectance.

3.1. Contribution Functions

[11] The concept of contribution function was used by *Dave and Mateer* [1967] for studying the possibility of estimating total atmospheric ozone from satellite measurements. In their study, they examined the contribution to the upward radiance for both primary scattering (single scattering) and all orders of scattering (multiple scattering). Photons that contribute from an atmospheric layer to the upward radiance may originate from other layers owing to multiple scattering, and the contribution function provides a measure of relative importance of each vertical layer in contributing to the upward radiation for a given atmospheric condition [see *Dave and Mateer*, 1967, Figure 2]. A concept similar to the contribution function is the weighting function introduced by *Platnick* [2000] for studying multiple scattering photon transport in cloud remote sensing. In the present study, the contribution function from different layers is extended to account for contributions from each individual scattering species, as described below.

[12] To calculate the contribution from each species in each layer we use the local estimate method [*Marchuk et al.*, 1980; *Evans and Marshak*, 2005]. The Monte Carlo scheme simulates photon trajectories, tracking where each scattering event occurs and what type of scattering species is involved using statistical methods. For given optical properties of the atmosphere this method computes contributions from each scattering species in each layer from each scattering event in the multiple scattering processes. In an atmosphere of N layers ($0 = z_0 < z_1 < \cdots < z_N = z_{TOA}$) the TOA reflectance, $R(x, y)$ is

$$R(x,y) = \sum_{k=1}^{N} \left(r_a(x,y,z_k) + r_m(x,y,z_k)\right) + r_s(x,y), \quad (1)$$

where $r_a(x, y, z_k)$ is the contribution from aerosols, $r_m(x, y, z_k)$ is the contribution from molecules in layer k, and $r_s(x, y)$ is the contribution from surface.
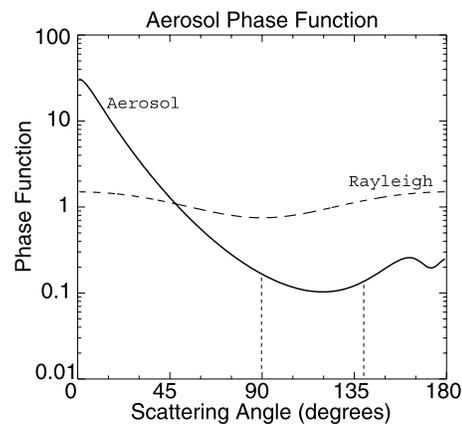
Figure 3. Aerosol phase function (solid line) as compared with the molecular Rayleigh phase function (dashed line) similar to those in Figure 6.3 of *Thomas and Stamnes* [1999]. Scattering angles θ for cloud-induced diffuse light (see Figure 2) below clouds ($\sim 90°$ to $\sim 140°$) are indicated.

[13] To illustrate the difference between single scattering and multiple scattering, we show examples for reflectance and associated partitions in clear atmospheric conditions. We performed a series of computation for a solar zenith angle of 30° with molecular and aerosol properties described in section 2 and surface albedos of 0.01 and 0.02 for wavelengths 0.47 μm and 0.66 μm, respectively. The single scattering accounts for a large portion ($\sim$72%) of reflected radiation at 0.47 μm and an even larger fraction ($\sim$83%) of total reflectance at 0.66 μm.

[14] For 0.47 μm, the partition of reflected radiation (surface, aerosol, molecule) is (0.066, 0.095, 0.839) for single scattering as compared to (0.065, 0.154, 0.781) for multiple scattering. For 0.66 μm, the partition of reflected radiation for (surface, aerosol, molecule) is (0.397, 0.167, 0.436) for single scattering versus (0.370, 0.220, 0.410) for multiple scattering. From single scattering to multiple scattering, an increase in contribution about 0.05 from aerosols (for both wavelengths) and associated decrease of contribution from molecular scattering contribution ($\sim$0.06 for 0.47 μm, $\sim$0.03 for 0.66 μm) are evident. The increase in aerosol contribution is because a large fraction of aerosols is in the lowest region of the atmosphere (see Figure 2b) where multiple scattering occurs more. This is similar to what was found by *Dave and Mateer* [1967] (see their Figure 2). A decrease of contribution from surface for both wavelengths is a result of blockage of surface reflected radiation by the atmosphere. Partitions of contributions from the Monte Carlo method capture additional contribution due to multiple scattering effects. Note that *Kaufman et al.* [1997a] partitioned the path radiance into the path radiance due to molecular scattering, and the path radiance due to aerosol scattering using single scattering partition. Here we include multiple scattering in computing the contribution to TOA reflectance.

3.2. Contribution to the Enhancement

[15] To study cloud effects on reflectance in nearby clear regions, we compute the effective contribution functions for cloudless atmosphere and 3D atmosphere with clouds and examine the differences between them. First we define cumulative contribution functions. In an atmosphere of N layers ($0 = z_0 < z_1 < \cdots < z_N = z_{TOA}$), the cumulative contribution at an altitude z_M represents the contribution from the layers below z_M, and is defined as

$$C_a(x,y,z_M) = \sum_{k=1}^{M} r_a(x,y,z_M) \qquad (2a)$$

$$C_m(x,y,z_M) = \sum_{k=1}^{M} r_m(x,y,z_k), \qquad (2b)$$

where $C_a(x, y, z)$ and $C_m(x, y, z)$ are cumulative contributions from aerosol and molecular scattering to the total outgoing radiance. For consistent notation, $C_s(x, y)$ is used for the surface contribution,

$$C_s(x,y) = r_s(x,y). \qquad (2c)$$

The TOA reflectances for cloudless atmosphere and 3D atmosphere are summations of contributions from each layer and from each type of scatterers as follows:

$$R_{1D} = \sum_{k=1}^{N} (r_a(z_k) + r_m(z_k)) + r_s$$
$$= C_{a,1D}(z_{TOA}) + C_{m,1D}(z_{TOA}) + C_{s,1D} \qquad (3a)$$

$$R_{3D}(x,y) = \sum_{k=1}^{N} (r_a(x,y,z_k) + r_m(x,y,z_k)) + r_s(x,y)$$
$$= C_{a,3D}(x,y,z_{TOA}) + C_{m,3D}(x,y,z_{TOA}) + C_{s,3D}(x,y). \qquad (3b)$$

[16] Having cumulative contributions defined in equations (2a)−(2c), we further define the cumulative contribution to the enhancement (CCE) as the difference between the contribution in the 3D atmosphere and its counterpart in the cloudless atmosphere, normalized by the total enhancement of the reflectance $\Delta R(x, y)$ at the top of the atmosphere (i.e., $\Delta R(x, y) = R_{3D}(x, y) - R_{1D}$) as follows:

$$\delta C_a(z) = \frac{\overline{C_{a,3D}(x,y,z)} - C_{a,1D}(z)}{\overline{\Delta R(x,y)}}, \qquad (4a)$$

$$\delta C_m(z) = \frac{\overline{C_{m,3D}(x,y,z)} - C_{m,1D}(z)}{\overline{\Delta R(x,y)}}, \qquad (4b)$$

$$\delta C_s = \frac{\overline{C_{s,3D}(x,y)} - C_{s,1D}}{\overline{\Delta R(x,y)}}, \qquad (4c)$$

where overbars indicate the horizontal average. δC_s, $\delta C_a(z)$, and $\delta C_m(z)$ are contributions to the reflectance enhancement from surface, aerosol, and molecular Rayleigh scattering from layers below z. $\delta C(z_2) - \delta C(z_1)$ is the contribution from a layer between z_1 and z_2.

4. Results

[17] The CCE is useful to demonstrate the contribution from different scattering species as a function of altitude, as well as the surface contribution. By comparing relative contributions from scattering species in each layer and from the surface, we will show that molecular scattering above clouds is the major physical mechanism responsible for the cloud-induced reflectance enhancement. We will further discuss the physics that leads to this conclusion. In section 4.1, we first examine CCE in clear regions in two cumulus cloud fields over dark surfaces and given aerosol optical thicknesses. In section 4.2, we examine the sensitivity of the CCE of molecular scattering and the total enhancement to the surface albedo and aerosol optical thickness.

4.1. Vertical Distribution of Contribution to the Enhancement

[18] It is worthwhile to briefly review some typical features of the enhancement of reflected radiation in clear regions in a cumulus cloud field. The enhancement of the
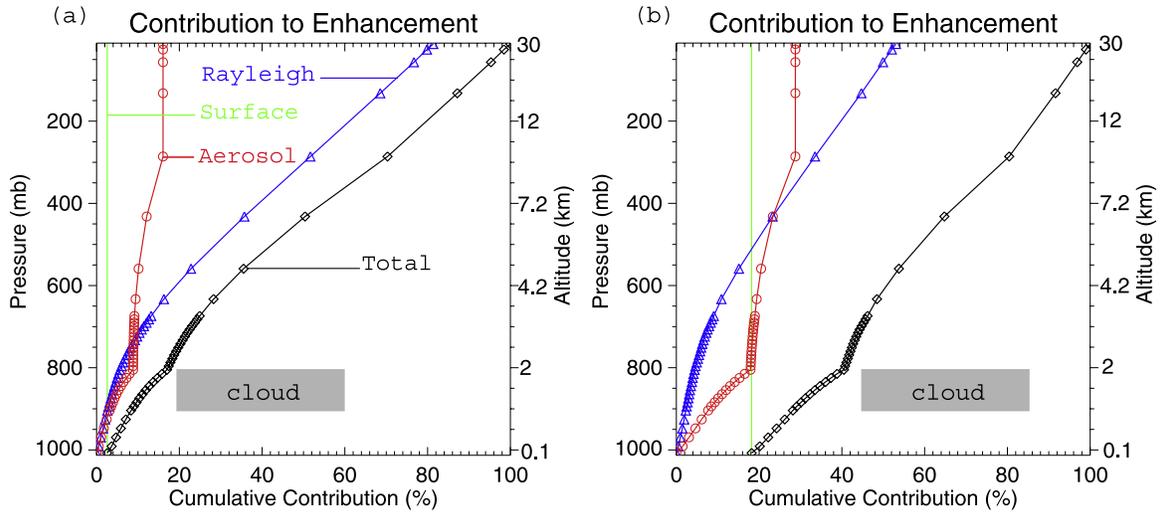
Figure 4. CCE for clear regions (1 km away from clouds) in the thick cumulus scene (Figure 1a) for SZA = 32° with cloud position indicated: (a) 0.47 μm and (b) 0.66 μm. Lines with circles are for CCE from aerosol scattering; lines with triangles are for CCE from Rayleigh scattering; straight lines are for CCE from surface contribution; lines with diamonds are the sums of all contributions to the enhancement. Molecular Rayleigh scattering contributes 82% and 52% to the TOA reflectance enhancements at 0.47 μm and 0.66 μm, respectively. The total reflectance enhancement due to clouds is 0.019 for 0.47 μm and 0.008 for 0.66 μm.

clear region reflectance has large variability near cloud edges, with strong enhancement in the sunlit side and small enhancement (often negative) over cloud shadows. The enhancement becomes less variable at about 1 km away from cloud edges [see *Wen et al.*, 2007, Figure 12]. To avoid large variations, we focus on clear regions 1 km away from cloud edges in this study. The CCE presented in the following is horizontally averaged excluding cloud shadowed and illuminated areas, for thick and thin cloud scenes. Cloud shadowed and illuminated areas are identified on the basis of large reflectance variability in a belt of about 1 km in width next to cloud edges [see *Wen et al.*, 2007, Figures 11 and 12]. To focus on the vertical distribution of the contribution, we assume the aerosol optical thickness is 0.2 at 0.47 μm and 0.1 at 0.66 μm (Figure 2b). The surface albedo is 0.01 for 0.47 μm and 0.02 for 0.66 μm. Sections 4.1.1 and 4.1.2 present results for SZA = 32° for thick and thin cloud scenes. Section 4.1.3 shows results for a lower solar elevation, namely SZA = 60°.

4.1.1. Contributions From Thick Clouds

[19] Figures 4a and 4b show CCE (equations (4a)–(4c)) for clear regions in the thick cloud scene (Figure 1a) at wavelengths of 0.47 μm and 0.66 μm, respectively. The surface contribution and vertical distributions of CCE for aerosol, molecular scattering, together with the summation of three components are plotted separately for both wavelengths. The relative contribution from surface, which is independent of altitude, is plotted as a straight vertical line. The pressure in vertical axis is proportional to molecular scattering optical thickness (Figure 2b). We discuss results in clear gaps in the boundary layer and the free troposphere [*Stull*, 1988] below and above cloud top height.

[20] For 0.47 μm (Figure 4a), the surface contribution is very small ($\delta C_s \sim 2\%$). Aerosols contribute $\delta C_a(z_{TOA}) \sim 16\%$ and molecular Rayleigh scattering contributes $\delta C_m(z_{TOA}) \sim$

82% to the total reflectance enhancement $\sim$0.019 at the TOA. Out of the total molecular contributions, about 90% (i.e., $\delta C_m(z_{TOA}) - \delta C_m(z_{cloud,top})$) is from the free troposphere.

[21] For 0.66 μm (Figure 4b), the surface, aerosol, and molecular Rayleigh scattering contribute $\delta C_s \sim 18\%$, $\delta C_a(z_{TOA}) \sim 29\%$ and $\delta C_m(z_{TOA}) \sim 53\%$, respectively, to the total reflectance enhancement of $\sim$0.008 at the TOA. Again we see that out of the total contribution of molecular Rayleigh scattering, about 90% is from the free troposphere.

[22] The CCE have distinctive features in the boundary layer and the free troposphere (Figures 4a and 4b). For molecules, the increase of CCE is much faster in the free troposphere as compared to in the boundary layer. Aerosol contribution is mainly from the boundary layer where most of the aerosols exist. Although, aerosol optical thickness is significantly larger than molecular scattering optical thickness in the boundary layer, aerosols contribute a small fraction to the reflectance enhancement. In the following part of this section we discuss the physics for the contributions from the two layers.

[23] The single scattering approximation is often used to illustrate physical processes in aerosol studies [e.g., *Kaufman et al.*, 1997a; *Remer et al.*, 2005]. Using the single scattering approximation one can easily illustrate that the contribution from a layer of clear atmosphere to the enhancement of the TOA reflectance (Δr) is proportional to the cloud diffuse radiance (F_{diff}), scattering optical depth of aerosols and molecules (τ) of the layer, and associated scattering phase function ($P(\theta)$) at the scattering angle θ,

$$\Delta r \sim F_{diff} \cdot \tau \cdot P(\theta). \qquad (5)$$

Thus cloud diffuse radiation, scattering optical thickness of aerosols and molecules, and associated phase function are

Contribution to Enhancement
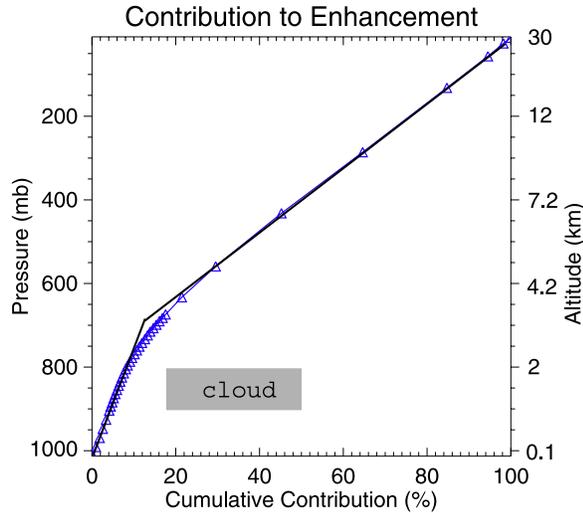
Figure 5. Same as the CCE in Figure 4 but for a molecular atmosphere with no aerosols and surface reflection for 0.47 μm (line with diamonds). Two straight lines schematically show the two vertical distinctive layers in clear areas near clouds. The total reflectance enhancement due to clouds is ~0.018.

the three major factors that determine contributions from each layer to the atmosphere TOA reflectance enhancement.

[24] Before making further discussions, we want to show that the cloud diffuse radiation in clear gaps of the boundary layer is significantly smaller than that in the free troposphere above. To illustrate this point we computed the CCE for molecular atmosphere with no aerosols and surface reflection (Figure 5). CCE are linear functions of pressure or molecular scattering optical thickness in the two layers. (Note molecular scattering optical thickness is proportional to the pressure.) However, the rate of increase of the CCE in the boundary layer is much smaller than that in the free troposphere. Since the molecular scattering phase function depends weakly on scattering angle, a slower rate of increase of the CCE in the boundary layer implies a smaller cloud diffuse radiation compared to that in the free troposphere. One can further estimate the relative strength of diffuse radiation in the two layers. Assuming a constant phase function in equation (5), one can derive

$$F_{diff}(below) \sim \frac{\Delta r(below)}{\Delta r(above)} \frac{\tau(above)}{\tau(below)} \cdot F_{diff}(above), \qquad (6)$$

where "below" and "above" indicate the boundary layer and the free troposphere below and above cloud top height, respectively. Using relative contributions and molecular optical thicknesses of the two layers ($\Delta r(below) \sim 8\%$, $\Delta r(above) \sim 92\%$ $\tau(below) \sim 0.037$, $\tau(above,) \sim 0.148$ at 0.47 μm), one can see that the average diffuse radiation in the boundary layer is about 1/3 of that in the free troposphere.

[25] For boundary layer clouds with a cloud top height ~2 km (or ~800 mb), molecular Rayleigh scattering optical thickness above the cloud top height is about 80% of the total molecular scattering optical thickness, considerably

larger than background aerosol optical thickness. Thus, the molecular Rayleigh scattering dominates the contribution to the enhancement of clear region reflectance in this layer.

[26] In the boundary layer, photons transmitted through cloud base or scattered from cloud sides are scattered by aerosols and molecules to enhance the clear regions reflectance. This radiation contributes only a small fraction to the TOA reflectance owing to the following factors: (1) the cloud diffuse radiation is small, only about 1/3 of that above clouds; (2) molecular scattering optical thickness is small; (3) aerosol phase function reaches minimum values of about 1 order of magnitude smaller than that for Rayleigh scattering (Figure 3). Using equation (5), the fact that aerosol scattering phase function is 1 order of magnitude smaller than Rayleigh scattering phase function, and the computed cloud diffuse radiation ratio, one can show that the contribution from the free troposphere is considerably larger than that from the boundary layer for given aerosol optical thickness at the two wavelengths. For aerosol optical thickness of 0.2 at 0.47 μm, the contribution to the reflectance enhancement from the free troposphere is about 8 times that from the boundary layer. For aerosol optical thickness of 0.1 at 0.66 μm, the contribution to the reflectance enhancement from the free troposphere is about 6 times that from the boundary layer.

[27] For a dark surface, the contribution to the enhancement is small. Since molecular Rayleigh scattering is weaker for longer wavelengths and contributes less to the total enhancement, the percentage contribution from the surface is expected to be larger for the longer wavelength as compared to the shorter wavelength.

4.1.2. Contributions From Thin Clouds

[28] The enhancement at the TOA is smaller in the thin cloud scene (Figure 1b) as compared to that in the thick cloud scene (Figure 1a) for both wavelengths. At 0.47 μm the cloud-induced enhancement in clear regions of thin cloud scene is ~0.012 as compared to ~0.019 in the thick cloud scene; and at 0.66 μm the enhancement is ~0.005 for the thin cloud scene compared to ~0.008 in the thick cloud scene. However, CCE for the thin cloud scene are similar to those for thick cloud scene with some exceptions. There are small decreases (~4% at 0.47 μm and ~7% at 0.66 μm) in molecular Rayleigh scattering contribution for the thin cloud scene as compared to the thick cloud scene. From thick to thin cloud scene, contributions from aerosols increase slightly (~3%) for both wavelengths; contributions from surface increase by ~1.5% at 0.47 μm and ~6% at 0.66 μm.

[29] Though the contribution from molecular Rayleigh scattering is a little less as compared to that in the thick cloud fields, it is still the major mechanism to the reflectance enhancements in clear regions in the thin cloud fields.

4.1.3. Contributions for Low Solar Elevation

[30] Sections 4.1.1 and 4.1.2 examine contributions to the enhancement of clear region reflectance in the vicinity of clouds for a specific SZA of 32° when images were acquired. It is useful to examine the contributions for a lower solar elevation for the interest of understanding the radiative processes for alternative situations. Here we demonstrate the results for a SZA of 60° to examine the solar angle dependence of the enhancement.
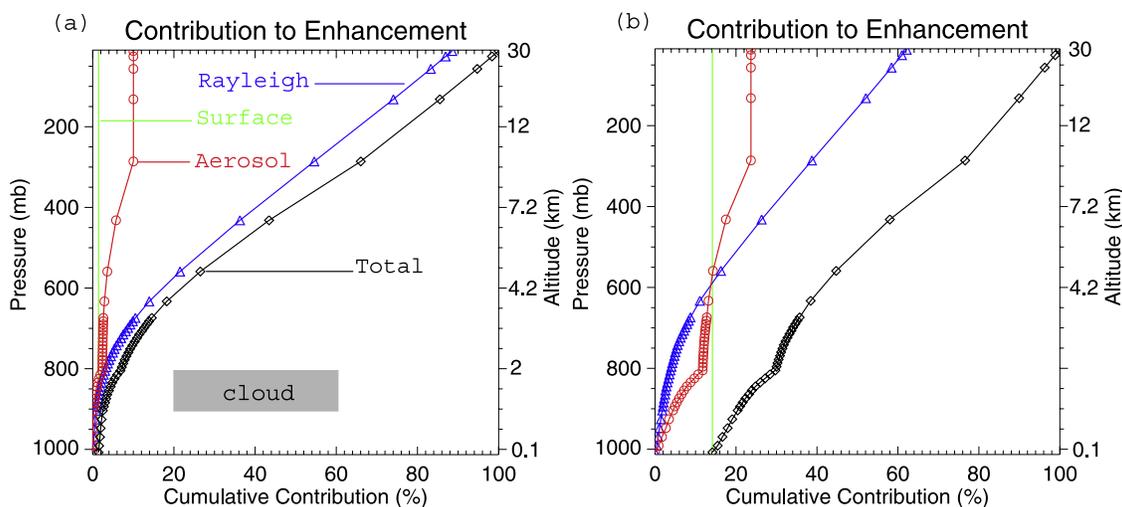
Figure 6. Similar to Figure 4 but for solar zenith angle of 60°. The CCE for clear regions (1.8 km away from clouds) in the thick cumulus scene (Figure 1a): (a) 0.47 μm and (b) 0.66 μm. The molecular Rayleigh scattering contributes ~90% and ~62% to the TOA reflectance enhancements at 0.47 μm and 0.66 μm, respectively. The total reflectance enhancements are 0.02 for 0.47 μm and 0.009 for 0.66 μm.

[31] A lower sun casts longer cloud shadow. For a cloud with a base height of 1 km, cloud shadows are ~1.73 km long from cloud edges for SZA of 60° (cloud height times tan(SZA)). For the thick cloud scene, the enhancement reaches the "asymptotic values" [*Wen et al.*, 2006] at a distance about 1.8 km away from cloud edges for thick clouds. For the thin cloud scene, clear areas excluding shadowed and sunlit pixels are considerably smaller than those in the thick cloud scene (see Figure 1b). Only a few pixels are not affected by either the sunlit side illumination effect or shadowing effect. Therefore, we only consider the thick cloud scene (Figure 1a) for the low solar elevation study.

[32] In clear regions in the thick cloud scene (Figure 1a), the total enhancement for low solar elevation is slightly larger than that for high solar elevation for the two wavelengths. From the high sun (SZA = 32°) to the low sun (SZA = 60°), the total reflectance enhancement increases by ~0.001 for both wavelengths, or ~5% and ~12% for 0.47 μm, and 0.66 μm, respectively.

[33] CCE in clear regions of the thick cumulus scene for SZA of 60° for the same aerosol, cloud, and surface properties (Figure 6) are similar to those for the high solar elevation (Figure 4). The same physical mechanisms for high solar elevation apply to interpret the vertical distribution of contributions. One can see that molecular Rayleigh scattering contributes $\delta C_m(z_{TOA}) \sim 89\%$ for 0.47 μm and $\delta C_m(z_{TOA}) \sim 62\%$ for 0.66 μm to the TOA enhancement. More than 90% of molecular Rayleigh scattering contributions are from the atmosphere above cloud height. From the high sun to the low sun, an increase of ~6% in the relative contribution from molecular Rayleigh scattering is associated with decreases of the relative contribution from surface reflection (~1–2%) and aerosol scattering (~4–5%).

[34] Further computations are performed for a large range of solar zenith angles. For SZA from 0° to 60°, we found that the enhancement increases by ~10% and ~20% for 0.47 μm and 0.66 μm, respectively. Here we reiterate that

shadowed pixels and pixels near the illuminated side of cloud edges are excluded because the reflectance of those pixels is so variable [*Wen et al.*, 2007]. In fact, the MODIS aerosol algorithm effectively avoids those pixels by excluding fractions of darkest and brightest pixels [*Remer et al.*, 2005].

4.2. Dependences on Surface Albedo and Aerosol Optical Thickness

[35] Figure 7 shows the distribution of the total enhancement in the thick cloud scene as a function of aerosol loading and surface albedo for the two wavelengths. For bright surfaces, the enhancement decreases with aerosol optical thickness. This is because the surface contribution dominates the enhancement when the surface is bright. As aerosol optical thickness increases, radiation from the surface gets attenuated exponentially leading to a decrease in the enhancement. For dark surfaces, the enhancement depends weakly on aerosol loading particularly for 0.47 μm. For a given aerosol optical thickness, the enhancement depends on the surface albedo, and such dependence is stronger at the longer wavelength. It is interesting to note that enhancement becomes less dependent on the surface albedo as aerosol loading increases, particularly for the shorter wavelength. It is also interesting to see that the enhancement for 0.66 μm is larger than that for 0.47 μm when aerosol loading is small (e.g., aerosol optical thickness is 0.01) and the surface is bright (e.g., surface albedo is 0.4). This is due to a much less atmospheric attenuation at the longer wavelength compared to the shorter wavelength.

[36] Zooming in Figure 7 we examine the dependence of the cloud-induced enhancement on aerosol optical thickness for a black surface in more detail in Figure 8. For 0.47 μm, the cloud-induced enhancement increases slightly, reaching a maximum at an aerosol optical thickness of ~0.4, then decreases gradually. The cloud-induced enhancement weakly depends on aerosol amount. Similarly, the cloud-induced enhancement for 0.66 μm does not strongly depend
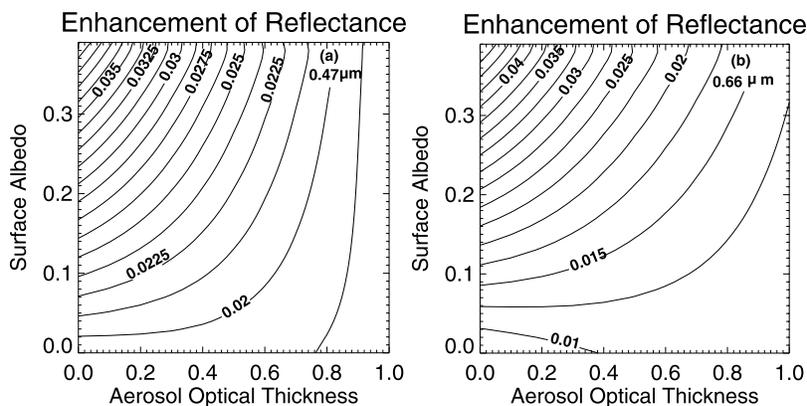
Figure 7. Total reflectance enhancement ($\Delta R = \overline{R_{3D}(x,y)} - R_{1D}$) in the thick cumulus scene as a function of aerosol optical thickness and surface albedo (a) 0.47 μm and (b) 0.66 μm.

on aerosol loading for aerosol optical thickness greater than 0.2. For 0.66 μm, although the relative change of the enhancement is large ($\sim$40%) for an increase of aerosol optical thickness from 0.01 to 0.2, the absolute change is about 0.002 corresponding to an overestimate of 0.02 in aerosol optical thickness. (One can show that the error in aerosol optical thickness due to the uncertainty in apparent reflectance is typically $\Delta\tau \sim 10\Delta R$ [e.g., *Kaufman et al.*, 1997b; *Wen et al.*, 1999]).

[37] An increase of aerosol optical thickness has two competing effects to the enhancement. First, an increase of aerosol optical thickness will result in a larger scattering optical thickness leading to an increase in the enhancement. When aerosol optical thickness continues to increase, the contrast between clouds and clear regions decrease. The smaller the contrast, the smaller the horizontal fluxes going from thicker to thinner areas leading to a decrease in the enhancement as discussed by *Marshak and Davis* [2005]. Nevertheless, it is evident that the magnitude of changes in the enhancement is small for a large range of aerosol optical thickness for both wavelengths.

[38] It is interesting to examine the fractional contribution from molecular Rayleigh scattering. Figure 9 shows the distribution of the fractional enhancement from molecular Rayleigh scattering to the total enhancement in Figure 7. It is evident that the fractional contribution from molecular Rayleigh scattering depends on surface albedo, aerosol amount, and wavelength. The brighter the surface, the more relative contribution is from the surface, and the less fractional contribution is from molecular Rayleigh scattering. For bright surfaces the fractional contribution from molecular Rayleigh scattering increases with aerosol optical thickness. Over the dark surface, molecular Rayleigh scattering contributes to a large portion of the enhancement. For 0.47 μm, the molecular Rayleigh scattering contributes $\sim$70–90% to the total enhancement for aerosol optical thickness up to 1. For 0.66 μm, the molecular Rayleigh scattering contributes $\sim$50% to the total enhancement for aerosol optical thickness up to $\sim$0.2.

[39] After examining the total enhancement and the fractional contribution from molecular Rayleigh scattering for a large range of surface albedo and aerosol loading, we conclude that the cloud-induced enhancement depends weakly on aerosol optical thickness over dark surfaces,

and molecular Rayleigh scattering is the major mechanism for the reflectance enhancement.

5. Summary and Discussions

[40] This paper employs a Monte Carlo scheme to examine physical mechanisms of radiative effects of boundary layer cumulus on enhancement of nadir reflectance in nearby clear regions for two ASTER images collocated with a MODIS scene in a biomass burning region of Brazil. We found that the scattering of radiation by clouds, followed by upward Rayleigh scattering by molecules above the cloud top over clear gaps is the dominant mechanism for cloud-induced enhancement of visible reflectance in clear regions over dark surfaces when aerosols are trapped in the boundary layer (see Figure 2). This result applies to thin and thick cloud scenes, and for high and low solar elevations. The mechanism is valid for a large range of aerosol optical thickness (up to 1 in this study) for 0.47 μm, and for aerosol optical thickness up to 0.2 for 0.66 μm.

[41] This finding provides simplifications for correcting cloud adjacency effects for remote sensing of aerosols in the vicinity of clouds, an important region for the understanding of cloud-aerosol interactions. Those simplifications are (1) details of aerosol loading and optical properties can be
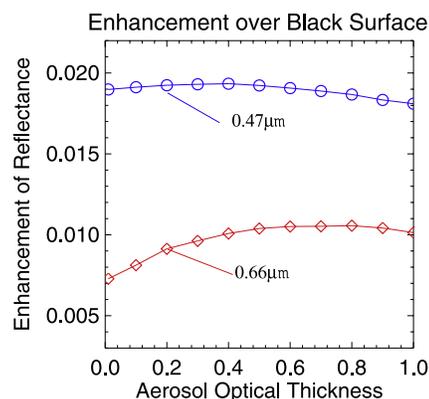
Figure 8. Total reflectance enhancement ($\Delta R = R_{3D} - R_{1D}$) over black surface from Figure 7 (line with circles for 0.47 μm; line with diamonds for 0.66 μm).
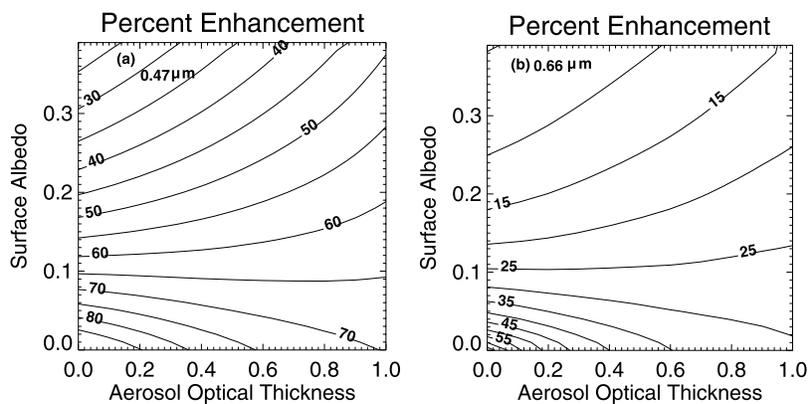
Figure 9. Distribution of the percent enhancement from molecular Rayleigh scattering in the thick cumulus scene as a function of aerosol optical thickness and surface albedo (a) 0.47 μm and (b) 0.66 μm. For dark surfaces, the molecular Rayleigh scattering contributes $\sim$50% to the total enhancement for aerosol optical thickness less than 0.2 at 0.66 μm. The molecular Rayleigh scattering contributes $\sim$70–90% to the total enhancement for aerosol optical thickness less than 1 at 0.47 μm.

neglected in computing cloud adjacency effects and (2) neglecting aerosol amount below clouds and accounting only cloud-Rayleigh radiative interaction may provide a good approximation for correcting 3D cloud adjacency effects particularly for shorter wavelengths [*Marshak et al.*, 2008]. The results apply to boundary layer clouds over dark surfaces. Those clouds preferably occur in subtropical eastern oceans, over the high-latitude oceans, and in regions of intense tropical convection, such as the Bay of Bengal during JJA and over the Amazon in Indonesia during DJF [*Hartmann et al.*, 1992]. Since "the largest contributions to net cloud forcing are provided by low clouds, especially in the tropical stratus cloud regions and the summer hemisphere" [*Hartmann et al.*, 1992], results of this work are significant to understanding aerosol-cloud interactions in such important regions.

[42] Since molecular scattering cross section has strong wavelength dependence and cloud albedo is almost wavelength independent in visible wavelengths, the cloud-induced enhancement of reflectance in clear regions of cloud scenes decreases with wavelength. For the same atmospheric conditions the reflected solar radiation in clear regions near clouds is more bluish compared to that in regions far away from clouds [*Marshak et al.*, 2008].

[43] In addition to absorbing aerosols with single scattering albedo of $\sim$0.9, we have also performed identical studies for nonabsorbing aerosols. We found that the results are similar for both absorbing and nonabsorbing aerosols. The enhancement is slightly larger (<5%) for the nonabsorbing aerosols as compared to absorbing aerosols over dark surfaces.

[44] We also found that the enhancement strongly depends on aerosol amount in the free troposphere above the cloud height. This is primarily due to the large increase of aerosol scattering phase function in the forward direction and available cloud diffuse radiation above clouds.

[45] Since molecular scattering above boundary layer clouds is the dominant mechanism for cloud-induced reflectance enhancement in clear regions near cloud edges, the complicated problem of aerosol-cloud radiative interactions can be simplified using a two-layer model to quantify the cloud-induced enhancement in clear regions of a cloudy atmosphere [*Marshak et al.*, 2008].

[46] However, this dominant physical mechanism is valid for boundary layer clouds above dark surface with a clean free troposphere above cloud top in visible wavelengths. Results of this study do not apply to all atmospheric conditions. Layers of dust aerosol at altitude above 3 km have been observed [e.g., *Kobayashi et al.*, 2003]. Smoke plumes can reach an altitude of 6 km [e.g., *Hoff et al.*, 2005]. Cirrus cloud at high altitude could potentially generate diffuse radiation to enhance the downward flux. Our results do not apply to convective clouds with large vertical extension. Since molecular scattering optical thickness in near infrared is much smaller than that in visible wavelengths, the molecular Rayleigh scattering in this region is no longer a dominant physical mechanism for near-infrared spectrum of solar radiation. All these situations are potentially important in satellite remote sensing of aerosols and require further research.

References

Cahalan, R. F., L. Oreopoulos, G. Wen, A. Marshak, S. C. Tsay, and T. P. DeFelice (2001), Cloud characterization and clear sky correction from Landsat 7, *Remote Sens. Environ.*, 78, 83–98, doi:10.1016/S0034-4257(01)00251-6.

Cahalan, R. F., et al. (2005), The International Intercomparison of 3D Radiation Codes (I3RC): Bringing together the most advanced radiative transfer tools for cloudy atmospheres, *Bull. Am. Meteorol. Soc.*, 86(9), 1275–1293, doi:10.1175/BAMS-86-9-1275.

Dave, J. V., and C. L. Mateer (1967), A preliminary study on the possibility of estimating total atmospheric ozone from satellite measurements, *J. Atmos. Sci.*, 24, 414–427, doi:10.1175/1520-0469(1967)024<0414: APSOTP>2.0.CO;2.

Evans, K. F., and A. Marshak (2005), Numerical methods in three-dimensional radiative transfer, in *Three-Dimensional Radiative Transfer in*

Cloudy Atmospheres, edited by A. Marshak and A. B. Davis, pp. 243–282, Springer, New York.

Hansen, J., and L. D. Travis (1974), Light scattering in planetary atmospheres, *Space Sci. Rev.*, 16, 527–610, doi:10.1007/BF00168069.

Hartmann, D. L., M. E. Ockert-Bell, and M. L. Michelsen (1992), The effect of cloud type on Earth's energy balance: Global analysis, *J. Clim.*, 5, 1281–1304, doi:10.1175/1520-0442(1992)005<1281:TEOCTO>2.0.CO;2.

Hoff, R. M., S. P. Palm, J. A. Engel-Cox, and J. Spinhirne (2005), GLAS long-range transport observation of the 2 003 California forest fire plumes to the northeastern US, *Geophys. Res. Lett.*, 32, L22S08, doi:10.1029/2005GL023723.

Ignatov, A., P. Minnis, N. Loeb, B. Wielicki, W. Miller, S. Sun-Mack, D. Tanre, L. Remer, I. Laslo, and E. Geier (2005), Two MODIS aerosol products over ocean on Terra and Aqua CERES SSF datasets, *J. Atmos. Sci.*, 62, 1008–1031, doi:10.1175/JAS3383.1.

Kassianov, E. I., and M. Ovtchinnikov (2008), On reflectance ratios and aerosol optical depth retrieval in the presence of cumulus clouds, *Geophys. Res. Lett.*, 35, L06807, doi:10.1029/2008GL033231.

Kaufman, Y. J., and I. Koren (2006), Smoke and pollution aerosol effect on cloud cover, *Science*, 313, 655–658, doi:10.1126/science.1126232.

Kaufman, Y. J., D. Tanre, L. A. Remer, D. Tanre, E. F. Vermote, A. Chu, and B. N. Holben (1997a), Operational remote sensing of tropospheric aerosol over land from EOS moderate resolution imaging spetroradiometer, *J. Geophys. Res.*, 102, 17,051–17,067, doi:10.1029/96JD03988.

Kaufman, Y. J., A. E. Wald, L. A. Remer, B.-C. Gao, R.-R. Li, and L. Flynn (1997b), The MODIS 2.1 mm channel-correlation with visible reflectance for use in remote sensing of aerosol, *IEEE Trans. Geosci. Remote Sens.*, 35, 1286–1298, doi:10.1109/36.628795.

Kaufman, Y. J., et al. (2005), A critical examination of the residual cloud contamination and diurnal sampling effects on MODIS estimates of aerosol over ocean, *IEEE Trans. Geosci. Remote Sens.*, 43, 2886–2897, doi:10.1109/TGRS.2005.858430.

Kobayashi, H., H. Fukushima, T. Murayama, Y. Hagihara, and S. Ohta (2003), Optical properties of Asian dust aerosol by SeaWiFS and contemporaneous ground observation data, *Proc. SPIE Int. Soc. Opt. Eng.*, 5155, 124, doi:10.1117/12.509460.

Koren, I., L. A. Remer, Y. J. Kaufman, Y. Rudich, and J. V. Martins (2007), On the twilight zone between clouds and aerosols, *Geophys. Res. Lett.*, 34, L08805, doi:10.1029/2007GL029253.

Loeb, N. G., and N. Manalo-Smith (2005), Top-of-atmosphere direct radiative effect of aerosols over global oceans from merged CERES and MODIS observations, *J. Clim.*, 18, 3506–3526, doi:10.1175/JCL13504.1.

Marchuk, G., G. Mikhailov, M. Nazaraliev, R. Darbinjan, B. Kargin, and B. Elepov (1980), *The Monte Carlo Methods in Atmospheric Optics*, 208 pp., Springer, New York.

Marshak, A., and A. B. Davis (2005), Horizontal fluxes and radiative smoothing, in *Three-Dimensional Radiative Transfer in Cloudy Atmospheres*, edited by A. Marshak and A. B. Davis, pp. 543–586, Springer, New York.

Marshak, A., G. Wen, J. A. Coakley, L. A. Remer, N. G. Loeb, and R. F. Cahalan (2008), A simple model for the cloud adjacency effect and the apparent bluing of aerosols near clouds, *J. Geophys. Res.*, 113, D14S17, doi:10.1029/2007JD009196.

Moody, E. G., M. D. King, S. Platnick, C. B. Schaaf, and F. Gao (2005), Spatially complete global spectral surface albedos: Value-added datasets derived from Terra MODIS land products, *IEEE Trans. Geosci. Remote Sens.*, 43, 144–158, doi:10.1109/TGRS.2004.838359.

Nikolaeva, O. V., L. P. Bass, T. A. Germogenova, A. A. Kokhanovsky, V. S. Kuznetsov, and B. Mayer (2005), The influence of neighboring clouds on the clear sky reflectance with the 3-D transport code RADUGA, *J. Quant. Spectrosc. Radiat. Transfer*, 94, 405–424, doi:10.1016/j.jqsrt.2004.09.037.

Platnick, S. (2000), Vertical photon transport in cloud remote sensing problems, *J. Geophys. Res.*, 105, 22,919–22,935, doi:10.1029/2000JD900333.

Platnick, S., M. King, S. Ackerman, W. P. Menzel, B. Baum, J. C. Riedi, and R. A. Frey (2003), The MODIS cloud products: Algorithms and examples from Terra, *IEEE Trans. Geosci. Remote Sens.*, 41, 459–473, doi:10.1109/TGRS.2002.808301.

Reid, J., P. V. Hobbs, R. J. Ferek, D. R. Blake, J. V. Martins, M. R. Dunlap, and C. Liousse (1998), Physical, chemical, and optical properties of regional hazes dominated by smoke in Brazil, *J. Geophys. Res.*, 103, 32,059–32,080, doi:10.1029/98JD00458.

Remer, L., Y. J. Kaufman, B. N. Holben, A. M. Thompson, and D. McNamara (1998), Biomass burning aerosol size distribution and modeled optical properties, *J. Geophys. Res.*, 103, 31,879–31,891, doi:10.1029/98JD00271.

Remer, L., et al. (2005), The MODIS aerosol algorithm, products, and validation, *J. Atmos. Sci.*, 62, 947–973, doi:10.1175/JAS3385.1.

Sekiguchi, M., T. Nakajima, K. Suzuki, K. Kawamoto, A. Higurashi, D. Rosenfeld, I. Sano, and S. Mukai (2003), A study of the direct and indirect effects of aerosols using global satellite data sets of aerosol and cloud parameters, *J. Geophys. Res.*, 108(D22), 4699, doi:10.1029/2002JD003359.

Stull, R. (1988), *An Introduction to Boundary Layer Meteorology*, 670 pp., Kluwer Acad., Norwell, Mass.

Thomas, G. E., and K. Stamnes (1999), *Radiative Transfer in the Atmosphere and Ocean*, 517 pp., Cambridge Univ. Press, Cambridge, U.K.

Wen, G., S. C. Tsay, R. Cahalan, and L. Oreopoulos (1999), Path radiance technique for retrieving aerosol optical thickness over land, *J. Geophys. Res.*, 104, 31,321–31,332.

Wen, G., R. F. Cahalan, S.-C. Tsay, and L. Oreopoulos (2001), Impact of cumulus cloud spacing on Landsat atmospheric correction and aerosol retrieval, *J. Geophys. Res.*, 106, 12,129–12,138, doi:10.1029/2001JD900159.

Wen, G., A. Marshak, and R. F. Cahalan (2006), Impact of 3D clouds on clear sky reflectance and aerosol retrieval in a biomass burning region of Brazil, *IEEE Geosci. Remote Sens. Lett.*, 3, 169–172, doi:10.1109/LGRS.2005.861386.

Wen, G., A. Marshak, R. F. Cahalan, L. Remer, and R. Kleidman (2007), 3D aerosol-cloud radiative interaction observed in collocated MODIS and ASTER images of cumulus cloud fields, *J. Geophys. Res.*, 112, D13204, doi:10.1029/2006JD008267.

Yang, Y., and L. Di Girolamo (2008), Impact of 3-D radiative effects on satellite cloud detection and their consequences on cloud fraction and aerosol optical depth retrievals, *J. Geophys. Res.*, 113, D04213, doi:10.1029/2007JD009095.

Zhang, J., J. S. Reid, and B. N. Holben (2005), An analysis of potential cloud artifacts in MODIS over ocean aerosol optical thickness products, *Geophys. Res. Lett.*, 32, L15803, doi:10.1029/2005GL023254.

R. F. Cahalan, A. Marshak, and G. Wen, NASA GSFC, Code 613.2, Greenbelt, MD 20771, USA. (Guoyong.Wen-1@nasa.gov)